INTERNATIONAL JOURNAL FOR NUMERICAL METHODS IN FLUIDS, VOL. 4, 1065–1081 (1984)

A COMPARISON OF MIXED METHODS FOR SOLVING THE FLOW OF A MAXWELL FLUID

J. J. VAN SCHAFTINGEN* AND M. J. CROCHET†

Unité de Mécanique Appliquée, Université Catholique de Louvain-la-Neuve, Bâtiment Stévin, 2 Place du Levant, B-1348 Louvain-la-Neuve, Belgium

SUMMARY

The proficiency of available mixed methods for solving the flow of a Maxwell fluid is evaluated through their application to the same problem. The reasons for the usual degeneracy of the numerical results beyond some level of elasticity are investigated. The best-performing technique is applied to the flow through an abrupt 4/1 contraction.

KEY WORDS Viscoelastic Fluids Polymer Flow Finite Elements

1. INTRODUCTION

The use of numerical techniques for solving the flow of viscoelastic fluids has known an intense development over the last few years; a review of the field has been given recently by Crochet and Walters,[1] who also give an extended list of references. A significant output of that activity has been the advent of numerous previously unsuspected problems which often prevent the attainment of a solution in the desired domain of elasticity. One may already anticipate that forthcoming developments on the field will need to deal with such difficult problems as velocity and stress boundary layers, and stress singularities of a still unknown intensity. Moreover, the selection of a constitutive equation, which has often been based on its proficiency in flows with simple kinematics, will need to be confronted with its consequences in complex flows.

In the present paper, we wish to consider the flow of fluids of the *differential type*, whose origin is closely associated with the name of Oldroyd;[2] briefly, the constitutive equations of such fluids consist of an algebraic tensorial relationship between the stress tensor, the rate of deformation tensor, and their time derivatives. One of the simplest, if not the easiest, representatives of that class is the upper-convected Maxwell fluid which has now served for many years as a model fluid for developing numerical techniques, and will be used as such in the present paper.

The main difficulty of using fluids of the differential type lies in the impossibility of obtaining an explicit representation of the stress tensor in terms of the derivatives of the velocity components. The general approach in numerical work, dating back to the papers by Kawahara and Takeuchi with finite elements[3] and by Perera and Walters[4] with finite differences, has been to use the stress components as unknowns together with the velocity components and the pressure (or the stream

* Aspirant, Fonds National de la Recherche Scientifique
† *All correspondence should be addressed to Prof. Crochet*

0271–2091/84/11 1065–17$01.70
© 1984 by John Wiley & Sons, Ltd.
Received 14 June 1983
Revised 24 October 1983

function and the vorticity). In finite element work, such a technique is proper to the so-called *mixed methods*, which have been used for quite some time in the u–v–p technique for solving the Navier–Stokes equations.

Several mixed finite element algorithms have been proposed for solving the flow of a Maxwell fluid; versions differing through the presentation of the basic equations and through the order of the shape functions may be found in References 5–9, where one tries to observe the effects of elasticity upon the flow. The elastic character of the flow is usually indicated by the group $\lambda V/L$, where λ is a relaxation time of the fluid, V is a characteristic velocity and L a characteristic length of the flow. Beyond some value of $\lambda V/L$ which depends upon the problem, the finite element mesh and the method, all the algorithms fail to converge towards a solution of the non-linear system. As long as one is satisfied with inspecting the sole streamlines, the lack of convergence seems rather brutal. However, a closer study of stress and velocity components before the break-up of convergence reveals the early appearance of premonitory wiggles well below the critical value of $\lambda V/L$.

Most problems of practical interest contain a stress singularity of unknown nature in viscoelastic flow, e.g. the re-entrant corner in an abrupt contraction, or the edge in the extrusion from a die. The stress singularity is obviously detrimental in a mixed method, especially when the stresses are represented by a continuous interpolation. In the present paper, we wish to consider a test problem of non-trivial kinematics, in the absence of stress singularities. A converging flow in a wedge, described in Section 3, satisfies these requirements. It is then possible to analyse the existing techniques, described in Section 2, and discover in Section 4 how they behave when they are confronted with the same problem. It will soon be found that their performance depends upon their ability to deal with the high stress gradients which are typical of many viscoelastic problems.

Further tests are presented in Section 5, based in particular on the use[10] of an Oldroyd-B fluid which allowed, in several problems, the attainment of relatively high values of $\lambda V/L$. It is then found that a method similar to the one used in Reference 9 for solving the flow of a second-order fluid should perform well for solving the flow of a Maxwell fluid; this is shown in Section 6, where the method is again used for solving the converging flow in a wedge. In Section 7, the method is then applied to the calculation of the flow of a Maxwell fluid in an abrupt axisymmetric 4/1 contraction. The algorithm behaves quite well before being apparently limited by high stress peaks at the re-entrant corner.

2. AVAILABLE MIXED METHODS FOR SOLVING THE FLOW OF A MAXWELL FLUID

Let $\boldsymbol{\sigma}$ denote the Cauchy stress tensor of an upper-convected Maxwell fluid; the fluid being incompressible, $\boldsymbol{\sigma}$ is decomposed as follows,

$$\boldsymbol{\sigma} = -p\mathbf{I} + \mathbf{T} \tag{1}$$

where p is the indeterminate pressure and $\mathbf{T}$ is the extra-stress tensor which is not traceless in general. Let $\mathbf{d}$ denote the rate of deformation tensor which is the symmetric part of the velocity gradient tensor $\mathbf{L}$; $\mathbf{T}$ satisfies the constitutive equation

$$\mathbf{T} + \lambda \overset{\nabla}{\mathbf{T}} = 2\mu\mathbf{d} \tag{2}$$

where λ is the relaxation time, μ is the (constant) shear viscosity, and a triangular superscript denotes the upper-convected, or contravariant, time-derivative

$$\overset{\nabla}{\mathbf{T}} = \partial\mathbf{T}/\partial t + \mathbf{v}\cdot\nabla\mathbf{T} - \mathbf{L}\mathbf{T} - \mathbf{T}\mathbf{L}^{\mathrm{T}} \tag{3}$$

The momentum equations are given by

$$-\nabla p + \nabla\cdot\mathbf{T} + \rho\mathbf{F} = \rho\mathbf{a} \tag{4}$$

where $\mathbf{F}$ is the body force per unit mass, ρ is the specific mass, and $\mathbf{a}$ is the acceleration. In the remainder of the paper, we will assume that $\mathbf{F}$ vanishes identically and that the inertia effects may be neglected, which is often the case in actual flows where viscoelasticity plays a dominant role. Moreover, we will limit ourselves to steady-state flows, for which $\partial\mathbf{T}/\partial t$ in (3) vanishes identically. Incompressibility requires that the velocity field be solenoidal, i.e.

$$\nabla\cdot\mathbf{v} = 0 \tag{5}$$

The problem now is to solve the set of non-linear partial differential equations consisting of (2), (4) and (5).

The basic difficulty is apparent in (2), where one finds that $\mathbf{T}$ cannot be expressed as an explicit tensor function of the velocity gradients; thus, for a Maxwell fluid, one cannot find the equivalent form of the Navier–Stokes equations by inserting the constitutive equations in the equations of motion. In dealing with the so-called differential form of the Maxwell fluid, it has been customary to introduce a mixed method, where the order of the system is reduced by the selection of the extra-stress tensor together with the velocity vector and the pressure as unknown variables. Typically, one defines a finite element representation as follows:

$$\tilde{\mathbf{T}} = \sum\mathbf{T}^{(i)}\phi_i, \tilde{\mathbf{v}} = \sum\mathbf{v}^{(i)}\psi_i, \tilde{p} = \sum p^{(i)}\pi_i \tag{6}$$

where $\mathbf{T}^{(i)}, \mathbf{v}^{(i)}$ and $p^{(i)}$ are nodal values and ϕ_i, ψ_i, π_i are the associated shape functions.

A first mixed method, which we call MIX1, is obtained through the application of the Galerkin formulation to (2), (4) and (5) as follows:

$$\langle\phi_i;\ \mathbf{T} + \lambda\overset{\nabla}{\mathbf{T}} - 2\mu\mathbf{d}\rangle = \mathbf{0} \tag{7a}$$

$$\langle(\nabla\psi_i)^{\mathrm{T}};\ -p\mathbf{I} + \mathbf{T}\rangle + \langle\psi_i;\ \rho\mathbf{a}\rangle = \mathbf{F}^{(i)} \tag{7b}$$

$$\langle\pi_i;\ \nabla\cdot\mathbf{v}\rangle = 0 \tag{7c}$$

For notational simplicity, we have used in (7) the original symbols $\mathbf{T}, \mathbf{v}$ and p instead of their interpolated counterparts in (6); $\mathbf{F}^{(i)}$ is the nodal vector force at the ith node which includes the contributions of the body forces and of the surface forces, and $\langle\ \rangle$ denotes the L^2 scalar product. It has been shown[5] that, with MIX1, the shape functions ϕ_i and ψ_i should be of the same order; here, we will adopt the representation given in Table I, which inevitably gives rise to a large number of nodal values.

When the relaxation time λ vanishes, the method MIX1 does not degenerate into the classical velocity–pressure formulation, which is known to provide an error $O(h^3)$ for the velocity components in Stokes flow. In order to obtain that formulation as a special case, and to allow for a representation of the extra stresses by means of polynomials of an order lower than those of the

Table I. Polynomial representations used with three mixed methods.

	Extra-stress	Velocity	Pressure
MIX1	P^2–C°	P^2–C°	P^1–C°
MIX2	P^2–C°	P^2–C°	P^1–C°
MIX3	P^1–C°	P^2–C°	P^1–C°

velocity components, one may introduce in the momentum equations the following decomposition:

$$\mathbf{T} = 2\mu\mathbf{d} - \lambda\overset{\nabla}{\mathbf{T}} \tag{8}$$

and write, instead of (7), the system

$$\langle \phi_i; \mathbf{T} + \lambda\overset{\nabla}{\mathbf{T}} - 2\mu\mathbf{d} \rangle = \mathbf{0} \tag{9a}$$

$$\langle (\nabla\psi_i)^{\mathrm{T}}; -p\mathbf{I} + 2\mu\mathbf{d} - \lambda\overset{\nabla}{\mathbf{T}} \rangle + \langle \psi_i, \rho\mathbf{a} \rangle = \mathbf{F}^{(i)} \tag{9b}$$

$$\langle \pi_i; \nabla\cdot\mathbf{v} \rangle = 0 \tag{9c}$$

Two mixed methods based on (9) are summarized in Table I; in the method MIX2 second degree polynomials are used for representing the velocity *and* the extra-stress components, whereas MIX3 uses second degree polynomials for the velocity components and first degree polynomials for the extra stresses.

The systems (7) and (9) give rise to a non-linear algebraic system in the nodal values of the velocity components, the extra-stress components and the pressure, which, in the present paper, is solved by Newton's method combined with an incremental procedure on the value of the relaxation time λ.

3. A TEST PROBLEM

The numerical techniques developed for solving the flow of viscoelastic fluids are typically applied for calculating the flow through an abrupt contraction or an extrusion die. The stress singularity at the re-entrant corner of the contraction or at the edge of the die renders such problems extremely difficult to solve; moreover, the nature of the singularity is unknown for the flow of a Maxwell fluid.

In order to avoid such difficulties which will be found again in Section 7, we will first compare the three mixed methods described in Section 2 by calculating the flow in a converging channel represented in Figure 1. The channel is a wedge with orthogonal walls. At a large distance from the tip of the wedge, where the extra stresses are small compared to their value near the tip, the inclined walls are connected to a plane channel which allows for a fully developed Poiseuille flow at the entry. Near the tip of the wedge, the walls are also connected to a plane channel by means of parabolic segments such that their equation is

$$x = \pm(1 + y^2/4), \quad -2 \leq y \leq 0 \tag{10}$$

The advantages of the parabolic walls for connecting the exit channel to the wedge are the absence of corners and the possibility of an exact geometrical representation by means of isoparametric elements.

The half-width of the downstream channel has a unit value, and the flow-rate for each half of the channel is also assumed to be one. The boundary conditions are indicated in Figure 1. The shear-rate on the downstream channel wall is denoted by $\dot{\gamma}_{\mathrm{W}}$, which takes the value 3 in the present problem. A measure of the elasticity of the flow is given by the product

$$S_{\mathrm{R}} = \lambda\dot{\gamma}_{\mathrm{W}} \tag{11}$$

The recoverable shear S_{R} is also the ratio of the first normal stress difference to twice the corresponding shear stress. In the present analysis, we will keep the flow-rate fixed and increase the value of λ, or S_{R}, in order to evaluate the effect of elasticity upon the flow.

At some distance from the tip of the wedge, it may be expected that, in the absence of inertia, the flow will be radial for a Newtonian fluid. It has been shown experimentally by Giesekus[11] that

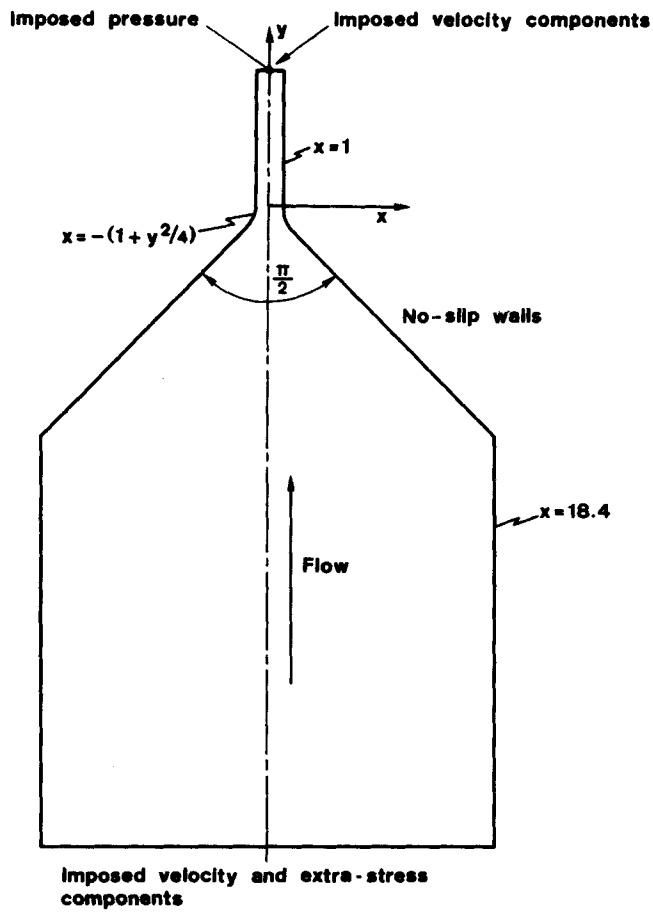

Figure 1. Plane converging channel and boundary conditions

some polymeric solutions would not follow the radial (Hamel) flow; on the contrary, one may expect under some circumstances a dramatic growth of vortices near the tip of the wedge. Within the (wide) range of elasticity covered by the present study, deviations from the radial flow will be hardly noticeable; however, the extra-stress field will be strongly affected by elasticity, along the curved part of the boundary in particular.

Several finite element meshes have been used for the present work; the elements used for constructing the meshes are nine-node Lagrangian quadrilaterals and six-node triangles. Having conducted several calculations on the mesh HAMEL 1 shown in Figure 2(a), we found it necessary to proceed to a local mesh refinement in the neighbourhood of the curved wall. Such a refined mesh, called HAMEL 2, is shown in Figure 2(b). However, it will be found in Section 4 that such a mesh is unsatisfactory. Thus, we constructed the mesh HAMEL 3, shown in Figure 2(c); here, the elements of HAMEL 1 have each been partitioned into four small elements. However, a part of the upstream domain has been omitted and the entry section is now a circular arc where one imposes the Newtonian velocity and a vanishing extra-stress field; this is a valid approximation at a large enough distance from the tip of the wedge. The characteristics of the meshes are summarized in Table II.

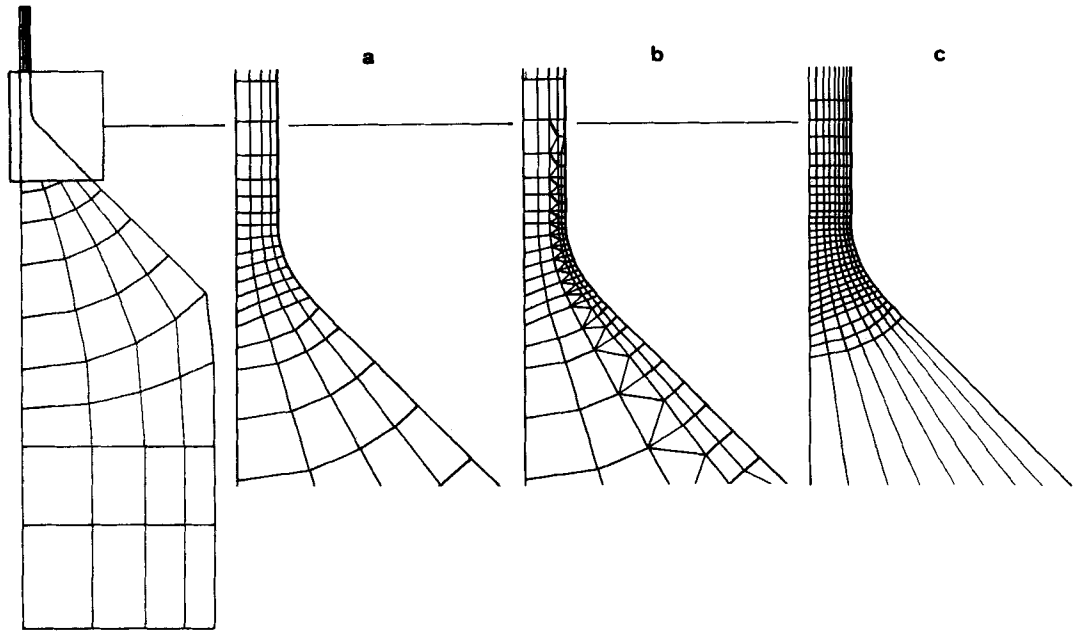

Figure 2. Finite element meshes used for calculating the flow in the domain shown in Figure 1: (a) HAMEL 1, (b) HAMEL 2, (c) HAMEL 3

Table II. Characteristics of the meshes shown in Figure 2

	HAMEL 1	HAMEL 2	HAMEL 3
Number of elements	116	204	240
Number of nodes	531	789	1037
Degrees of freedom: MIX1 and MIX2	2805	4164	5464
Degrees of freedom: MIX3	1662	2454	3190

4. NUMERICAL RESULTS

Let us first consider the Newtonian case calculated with the velocity–pressure formulation on the mesh HAMEL 1. Figure 3(a) shows a comparison of the calculated velocity component on the plane of symmetry in the y direction with the analytical value obtained in a Newtonian radial flow; the corresponding streamlines are shown in Figure 3(b). In order to anticipate the results which will be found when the flow becomes viscoelastic, it is instructive to study the extra-stress field on the wall. Let s denote a curvilinear coordinate along the wall of the contraction, and let n denote a coordinate along the normal to the wall. The velocity components vanish on the no-slip wall and, in view of the incompressibility of the fluid, the only non-vanishing velocity gradient on the wall is $\partial v_s/\partial n$, where v_s denotes the tangential velocity component. In a Newtonian flow, the shear-stress on the wall T_{ns} will therefore be the only non-vanishing extra-stress component on the wall. Figure 4 shows a plot of T_{ns} on the wall of the contraction as a function of the arc length s. The curve shows a slight overshoot near the entry to the plane channel, which may be related to the discontinuous curvature of the wall.

The overshoot of the shear-stress on the wall will have important consequences when the flow

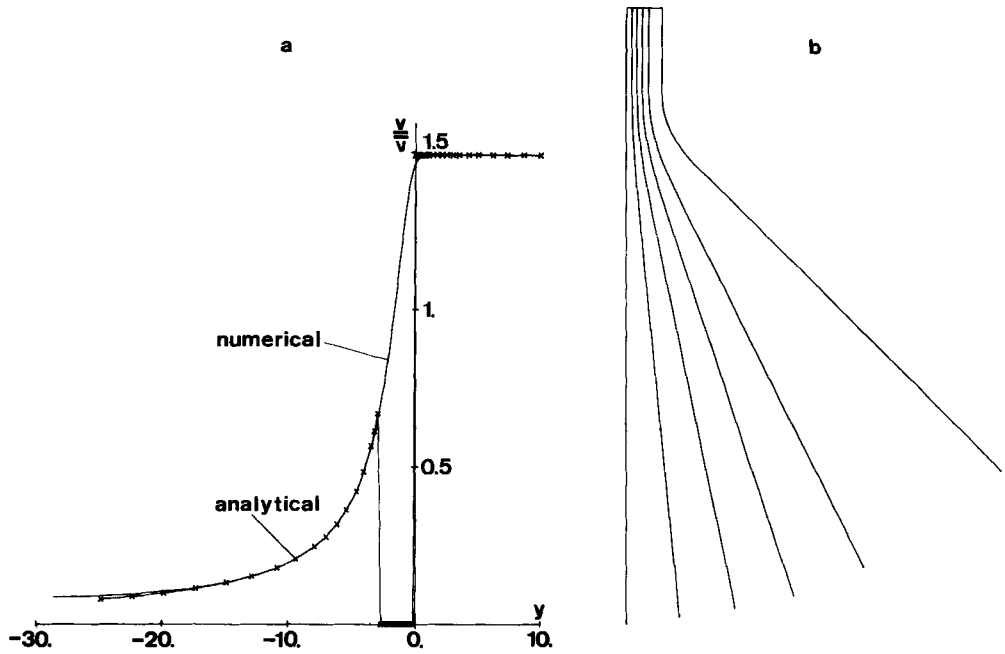

Figure 3. Newtonian solution on the mesh HAMEL 1: (a). numerical value of the velocity in the plane of symmetry compared with the analytical value in Hamel flow; (b) streamlines

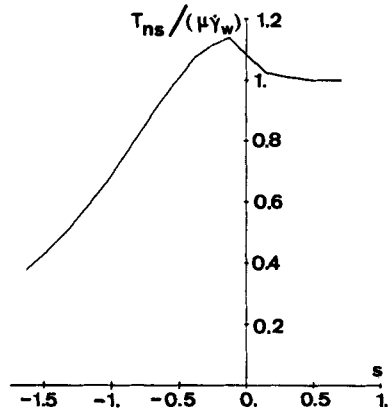

Figure 4. Graph of the tangential stress component T_{ns} on the wall

becomes viscoelastic. It is easy to show that the viscometric functions determine the extra-stresses on the wall in terms of the local shear-rate $\dot{\gamma}$. For the flow of a Maxwell fluid, one obtains

$$T_{ns} = \mu\dot{\gamma}, \quad T_{ss} = 2\lambda\mu\dot{\gamma}^2, \quad T_{nn} = 0 \tag{12}$$

Simply assuming that the Newtonian velocity field remains valid in a viscoelastic flow calculation, we may already expect that the overshoot in T_{ns} and $\dot{\gamma}$, will give rise to a much more important overshoot in T_{xx}, since T_{ss} contains the *square* of the shear rate and an amplifying factor λ. We will now find that the rapid variation of T_{ss} along the wall is the main difficulty of the present problem.

Table III. Dependence of the upper limit of convergence in S_R upon the mixed method, with the mesh HAMEL 1

Method	MIX1	MIX2	MIX3
Upper limit of S_R	4·75	3	7

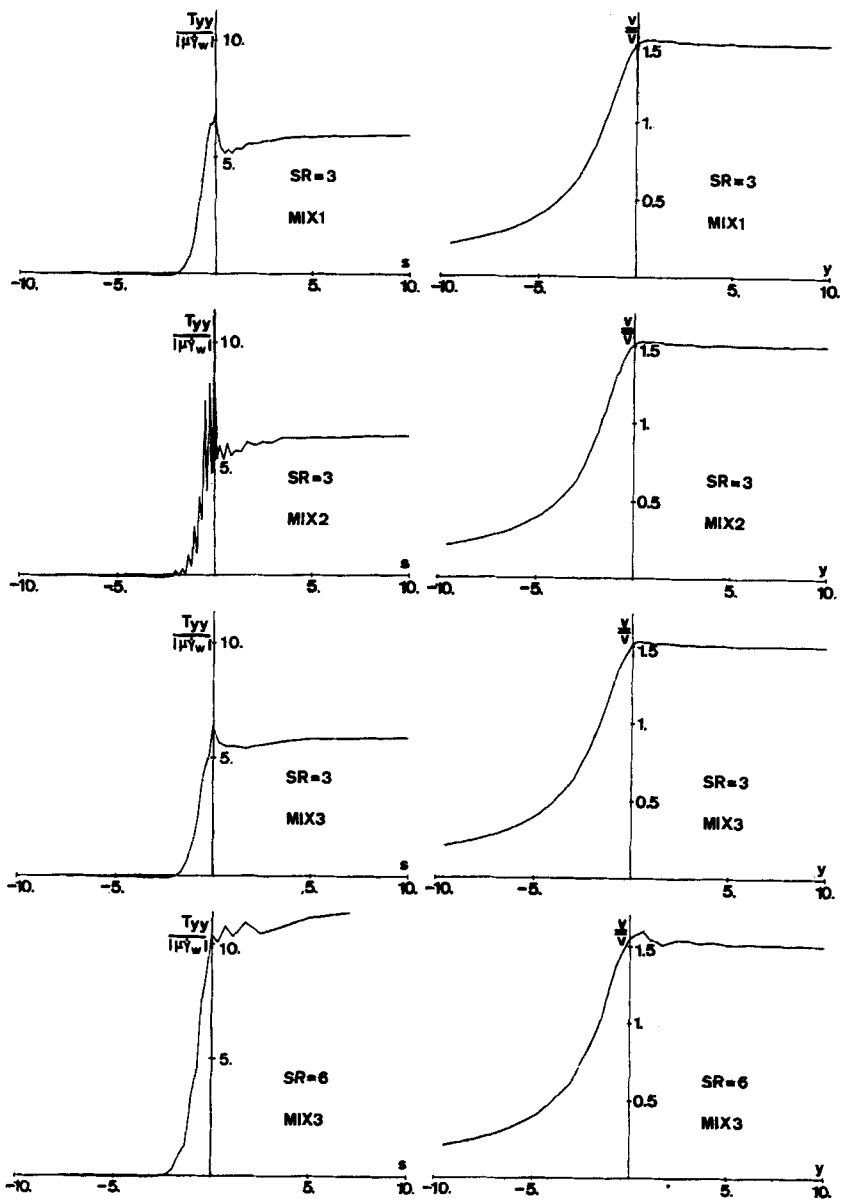

Figure 5. Graphs of the T_{yy} extra-stress component along the wall, and of the velocity on the plane of symmetry. The values of S_R and the method are indicated in the Figures

Table IV. Dependence of the upper limit of convergence in S_R upon the mesh refinement, with the method MIX3

Mesh	HAMEL 1	HAMEL 2	HAMEL 3
Upper limit of S_R	7	5	4·5

In most numerical viscoelastic flow calculations one finds that, beyond some value of the recoverable shear S_R, the solution degenerates and exhibits a spatial oscillatory pattern where one recognizes the size of the elements. For a higher value of S_R, Newton's method ceases to converge and the calculation blows up. It may however sometimes happen that the method blows up without the preliminary appearance of wiggles in the field variables.

The problem of the flow in the wedge has been run on the mesh HAMEL 1 with methods MIX1, MIX2 and MIX3; with the three methods, one may observe the development of wiggles followed by the lack of convergence of Newton's method. Table III gives the limit of S_R beyond which no solution could be found. The fact that the iterative method converges does not mean that the solution is acceptable. In order to show this, let us consider in Figure 5 two significant plots obtained with each method. On the left, we plot the extra-stress T_{yy} on the wall of the contraction against the arc-length s, and on the right we plot the ratio $v/\bar{v}$ of the y-velocity component on the plane of symmetry divided by the mean velocity, against the y co-ordinate, for the value $S_R = 3$. The stress peak which we had anticipated on the basis of the Newtonian solution is quite apparent on the diagrams showing T_{yy} as a function of s. With MIX1, the wiggles in the stress field announce the loss of convergence and the wild oscillations obtained with MIX2 indicate why no converged solution could be found beyond $S_R = 3$. In MIX3, the extra-stresses are approximated by means of first degree polynomials which do not allow for a clear-cut description of the stress overshoot and seem to delay the loss of convergence. The curve of T_{yy} at $S_R = 6$ obtained with MIX3 shows the development of wiggles. Slight oscillations are also apparent on the velocity profile along the plane of symmetry.

In view of the rapid rise of the extra-stresses along the wall, a natural reaction is to refine the finite element mesh with the hope of increasing the upper-limit of S_R. Therefore, the same calculation has been performed with MIX3 on the meshes HAMEL 2 and HAMEL 3. The limit values of S_R are reported in Table IV; it is troublesome to find that, as in many other problems, the limit of convergence decreases when the finite element mesh is refined, although it is not always the case. Such an odd behaviour is at present unexplained.

5. TENTATIVE DIAGNOSIS

In trying to understand the reason for the lack of convergence beyond some value of S_R, one may wonder whether the Galerkin formulation of the constitutive equations given by (7a) and (9a) is responsible for the rugged behaviour of the stress field. An easy answer is obtained to that question by introducing the *Newtonian* velocity field in (7a) or (9a); the extra-stress field is then retrieved for a given value of λ by solving the resulting linear system. Such a numerical experiment is interesting because it may tell us whether the convective terms contained in $\overset{\nabla}{\mathbf{T}}$ are responsible for the wiggles, by analogy with the inertia terms in the Navier–Stokes equations.

Let $\mathbf{v}^N$ be the Newtonian velocity field and $\mathbf{L}^N$, $\mathbf{d}^N$ the associated velocity gradients and rate of deformation tensors. In view of (3) and (7), we thus solve the following set of algebraic equations which is linear in the stress field,

$$\langle \phi_i; \mathbf{T} + \lambda[\mathbf{v}^N \cdot \nabla \mathbf{T} - \mathbf{L}^N \mathbf{T} - \mathbf{T}(\mathbf{L}^N)^T] - 2\mu \mathbf{d}^N \rangle = \mathbf{0} \tag{13}$$

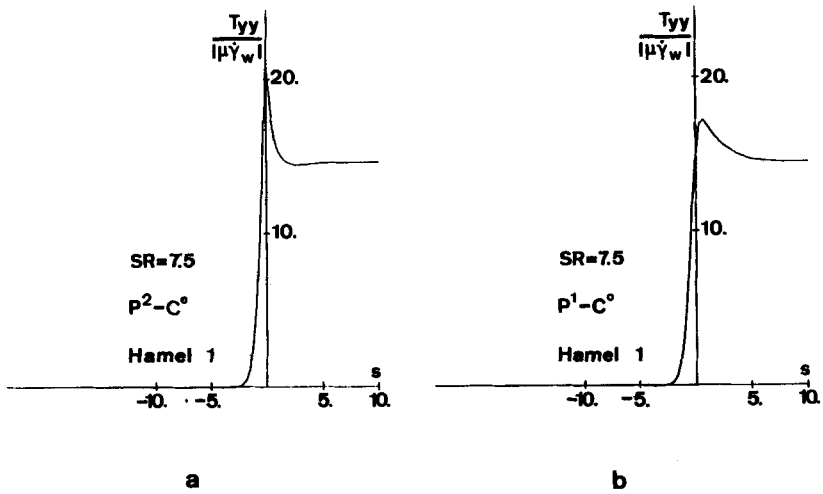

Figure 6. Extra-stress component T_{yy} along the wall obtained on the basis of the Newtonian velocity field and the mesh HAMEL 1: (a) P^2–C^0 interpolation; (b) P^1–C^0 interpolation

Figure 6(a) shows the graph of T_{yy} along the wall for $S_R = \lambda\dot{\gamma}_W = 7{\cdot}5$ when the interpolation for the extra-stresses is of the P^2–C^0 type, as in MIX1 and MIX2; Figure 6(b) corresponds to an interpolation of the P^1–C^0 type, proper to MIX3. Both curves have been obtained with the mesh HAMEL 1.

It is obvious that the wiggles have disappeared altogether. The use of a P^1–C° interpolation flattens the stress peak; this shows that a coarser interpolation leads in the present case to lower stress gradients, which might justify why the upper limit of S_R decreases when the mesh is refined.

Let us also consider the effect of a mesh refinement upon the calculation of the extra-stresses with a P^1–C^0 interpolation. Figure 7(a) shows the curve of T_{yy} on the wall obtained with the mesh HAMEL 2 shown in Figure 2; the spurious wiggles would tend to confirm that an irregular element pattern in a region of high stress gradients is very detrimental in a convective problem.

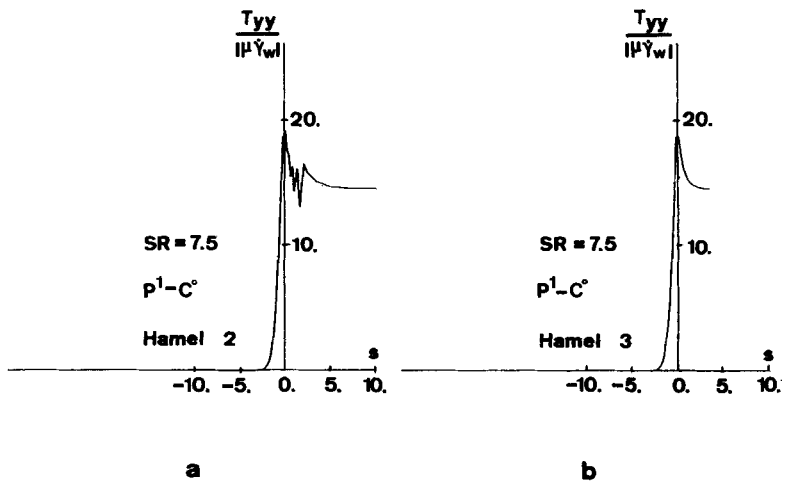

Figure 7. Extra-stress component T_{yy} along the wall obtained on the basis of the Newtonian velocity field and a P^1–C^0 interpolation: (a) mesh HAMEL 2; (b) mesh HAMEL 3

Figure 7(b) shows the curve of T_{yy} obtained with the mesh HAMEL 3, which is similar to HAMEL 1 except that all the elements have been divided into four smaller elements. The P^1–C^0 interpolation on HAMEL 3 should therefore be essentially the same as the P^2–C^0 interpolation on HAMEL 1. Figure 7(b), which is very similar to Figure 6(a), confirms that conjecture.

It is now clear that the Galerkin formulation of the constitutive equations may not be held responsible for the degeneracy of the numerical results; rather, one must investigate the coupling between the constitutive equations and the equations of motion. In that respect, it is worth returning briefly to the method proposed by Crochet and Keunings[10] for solving the flow of an Oldroyd-B fluid; the use of such a fluid gives rise to an important increase of the critical value of S_R beyond which the iterative technique does not converge.

The extra-stress tensor of an Oldroyd-B fluid may be written as follow:

$$\mathbf{T} = \mathbf{T}_1 + \mathbf{T}_2 \tag{14a}$$

$$\mathbf{T}_1 + \lambda \overset{\nabla}{\mathbf{T}}_1 = 2\mu_1 \mathbf{d} \tag{14b}$$

$$\mathbf{T}_2 = 2\mu_2 \mathbf{d} \tag{14c}$$

thus, $\mathbf{T}_1$ has a constitutive equation identical to (2), and $\mathbf{T}_2$ is purely viscous. After eliminating $\mathbf{T}_1$ and $\mathbf{T}_2$ from (14) one obtains

$$\mathbf{T} + \lambda \overset{\nabla}{\mathbf{T}} = 2(\mu_1 + \mu_2)(\mathbf{d} + \lambda^* \overset{\nabla}{\mathbf{d}}) \tag{15}$$

where $\lambda^* = \lambda\mu_2/(\mu_1 + \mu_2)$ is the *retardation time.*

The Oldroyd-B fluid and the upper-convected Maxwell fluid are indistinguishable on the basis of their viscometric functions; oscillatory experiments can in principle allow for the measurement of the retardation time.[12]

The form (15) of the constitutive equations is inconvenient for a numerical simulation, because $\overset{\nabla}{\mathbf{d}}$ contains second order partial derivatives of the velocity field. However, observing that

$$\mathbf{T} = 2\mu_2 \mathbf{d} + \mathbf{T}_1 \tag{16}$$

where $\mathbf{T}_1$ is given by (14b), one may easily transform the method MIX1 given by (7) in order to calculate the flow of an Oldroyd-B fluid and obtain

$$\langle \phi_i; \mathbf{T}_1 + \lambda \overset{\nabla}{\mathbf{T}}_1 - 2\mu_1 \mathbf{d} \rangle = \mathbf{0} \tag{17a}$$

$$\langle (\nabla \psi_i)^{\mathrm{T}}; -p\mathbf{I} + 2\mu_2 \mathbf{d} + \mathbf{T}_1 \rangle + \langle \psi_i; \rho \mathbf{a} \rangle = \mathbf{F}^{(i)} \tag{17b}$$

$$\langle \pi_i; \nabla \cdot \mathbf{v} \rangle = 0 \tag{17c}$$

The presence of a viscous term in the momentum equation, justified by the constitutive equations, completely transforms the behaviour of the algorithm. The method has been applied to the wedge problem with the mesh HAMEL 1, and with a viscosity ratio $\mu_1/\mu_2 = 8$; the algorithm is still converging at $S_R = 9$ but the calculation has not been pursued in view of the increasing amplitude of the wiggles. Figure 8 shows the results obtained for the extra-stress T_{yy} along the wall and for the vertical velocity component along the plane of symmetry at $S_R = 6{\cdot}2$, with a P^2–C° *interpolation* for the stress field. The same interpolation refinement of the stresses may be obtained with MIX3 (P^1–C^0) on the mesh HAMEL 3, but in that case Table IV shows that the algorithm could not converge beyond $S_R = 4{\cdot}5$, with the use of the upper-convected Maxwell fluid.

The results shown in the present and in the previous sections lead us to the following remarks:

(i) The Galerkin formulation of the constitutive equations and the associated convective terms does not appear to be *per se* the cause of the degeneracy of the solution, provided however that the finite element mesh is regular enough.

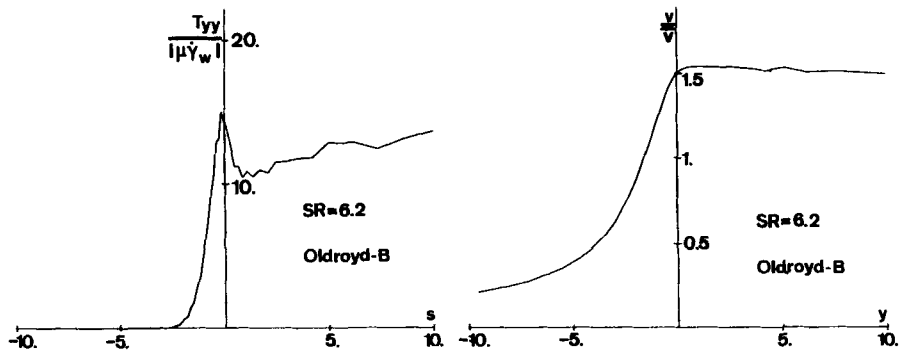

Figure 8. Graphs of the T_{yy} extra-stress component along the wall, and of the velocity on the plane of symmetry for an Oldroyd-B fluid

(ii) The stress-derivatives appearing in the form of the momentum equations proper to MIX2 and MIX3 seem to be detrimental.

(iii) The addition of a viscous component in the momentum equations, which is proper to the calculation of the flow of an Oldroyd-B fluid, produces an appreciable enlargement of the domain of convergence.

In the next section we will take these remarks into account for formulating another mixed method which would be suitable for calculating the flow of a Maxwell fluid.

6. ANOTHER MIXED METHOD

Our aim is to provide a mixed method where viscous terms are present in the equations of motion without however inserting partial derivatives of the extra stresses. A convenient approach is to introduce the following substitution for the extra-stresses:

$$\mathbf{T} = 2\mu\mathbf{d} + \mathbf{S} \tag{18}$$

The constitutive equation for $\mathbf{S}$ is then, on the basis of (2),

$$\mathbf{S} + \lambda\overset{\nabla}{\mathbf{S}} + 2\lambda\mu\overset{\nabla}{\mathbf{d}} = 0 \tag{19}$$

We may now use the following variables for defining an approximation:

$$\tilde{\mathbf{S}} = \sum \mathbf{S}^{(i)}\phi_i, \tilde{\mathbf{v}} = \sum \mathbf{v}^{(i)}\psi_i, \tilde{p} = \sum p^{(i)}\pi_i \tag{20}$$

The Galerkin formulation of (19) requires some care; indeed, the term $\langle \phi_i; \overset{\Delta}{\mathbf{d}} \rangle$ contains second-order spatial derivatives of the velocity components, and the use of a C^0-representation would lead to a non-conforming finite-element representation. However, using the divergence theorem, we obtain the following identity:

$$\begin{aligned} \langle \phi_i; \overset{\nabla}{\mathbf{d}} \rangle &= \langle \phi_i; \nabla\cdot(\mathbf{vd}) \rangle - \langle \phi_i; \mathbf{Ld} + \mathbf{dL}^{\mathrm{T}} \rangle \\ &= -\langle (\nabla\phi_i)^{\mathrm{T}}; \mathbf{vd} \rangle - \langle \phi_i; \mathbf{Ld} + \mathbf{dL}^{\mathrm{T}} \rangle + \langle\langle \phi_i; v_n\mathbf{d} \rangle\rangle \end{aligned} \tag{21}$$

where a double bracket represents a surface integral along the boundary of the domain.

A mixed method, which we will call MIX4, may thus be defined as follows,

$$\langle \phi_i; \mathbf{S} + \lambda\overset{\nabla}{\mathbf{S}} - 2\lambda\mu(\mathbf{Ld} + \mathbf{dL}^{\mathrm{T}}) \rangle - 2\lambda\mu\langle (\nabla\phi_i)^{\mathrm{T}}; \mathbf{vd} \rangle + 2\lambda\mu\langle\langle \phi_i; v_n\mathbf{d} \rangle\rangle = \mathbf{0} \tag{22a}$$

$$\langle (\nabla\psi_i)^{\mathrm{T}}; -p\mathbf{I} + 2\mu\mathbf{d} + \mathbf{S} \rangle + \langle \psi_i; \rho\mathbf{a} \rangle = \mathbf{F}^{(i)} \tag{22b}$$

$$\langle \pi_i; \nabla\cdot\mathbf{v} \rangle = 0 \tag{22c}$$

where v_n denotes the normal component of the velocity on the boundary. The first equation contains the flux of the rate of deformation tensor on the boundary of the flow domain. On rigid walls, v_n vanishes identically, and so does the flux of $\mathbf{d}$; the same is true on a plane or an axis of symmetry. In an entry section, the components of the tensor $\mathbf{S}$ are imposed as essential boundary conditions in view of the hyperbolic nature of the constitutive equations; the essential boundary conditions replace equation (22a). In an exit section, one may not in principle impose the value of $\mathbf{S}$; it is however possible to express the surface integral $\langle\langle \phi_i; v_n \mathbf{d} \rangle\rangle$ in terms of the nodal velocity components, and to replace it by a contribution to the non-linear algebraic system. When the exit section is long enough so that the flow is fully developed as the fluid leaves the flow domain, it has been found that imposing the value of $\mathbf{S}$ or expressing the surface integral in terms of nodal velocities lead to the same numerical solution.

The method MIX4 has been tested with a P^2–C^0 interpolation for the velocity components, and a P^1–C^0 interpolation for the components of $\mathbf{S}$ and the pressure. Let us consider in the present section the results obtained for the flow in a wedge described in Section 3. On the mesh HAMEL 1, the algorithm is still converging at $S_R = 7{\cdot}5$; moreover, the algorithm is still converging at $S_R = 7$ on HAMEL 3. The calculation has however been stopped in view of increasing wiggles in the stress field.

Figure 9 shows the results obtained at $S_R = 3$ and $S_R = 6$ with MIX4 on HAMEL 1; these results should be compared with those of Figure 5 obtained with MIX3, based on the same type of interpolation. The results obtained with MIX4 on the mesh HAMEL 3 exhibit a marked stress overshoot at the entry of the plane channel and are very similar to those obtained with an Oldroyd-B fluid, shown in Figure 8.

The method MIX4, which has just been shown to provide good performances for high values of S_R, is essentially the same as the method used by Mendelson *et al.*[9] for calculating the flow of a second order fluid. However, these authors disregarded the method for calculating the flow of a Maxwell fluid in view of its bad performances; our experience contradicts that evaluation.

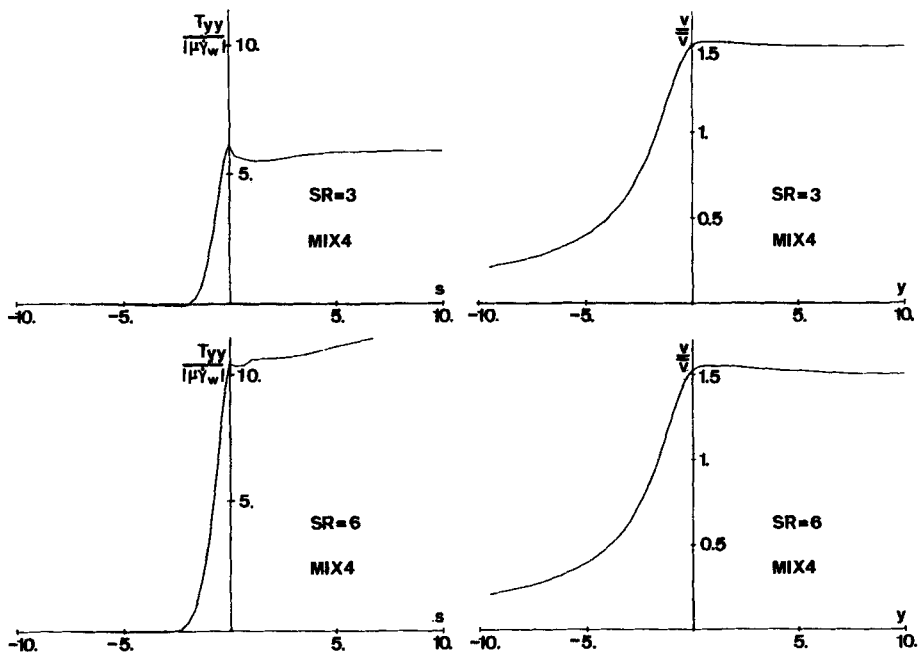

Figure 9. Graphs of the T_{yy} extra-stress component along the wall, and of the velocity on the plane of symmetry for a Maxwell fluid with the method MIX4

7. THE FLOW OF A MAXWELL FLUID THROUGH AN ABRUPT CONTRACTION

The flow of a viscoelastic fluid through an abrupt contraction has become a classic in view of its complexity combined with its intrinsic interest in experimental rheology. It is known indeed that some materials exhibit an important growth of the corner vortex when the elasticity of the flow increases, although some others do not provide any modification of the kinematics; it is hoped that the numerical simulation of the flow will provide a hint for understanding the observed phenomena. The flow of a Maxwell fluid through a 4/1 axisymmetric contraction was studied by Viriyayuthakorn and Caswell[13] who, using the integral representation of the Maxwell fluid, could obtain converged solutions up to $S_R = 2$; no significant vortex growth could be observed. This result has been confirmed by Crochet[14] who, using the Oldroyd-B model, reached a value of

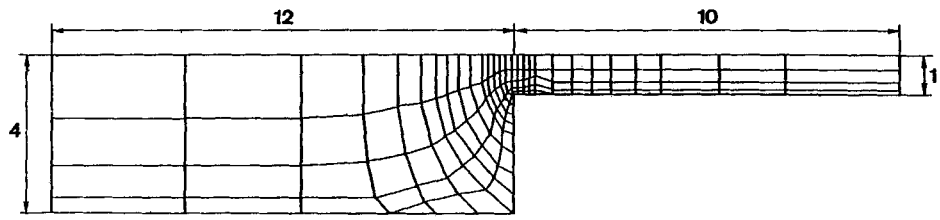

Figure 10. Finite element mesh for calculating the flow in an axisymmetric 4/1 contraction

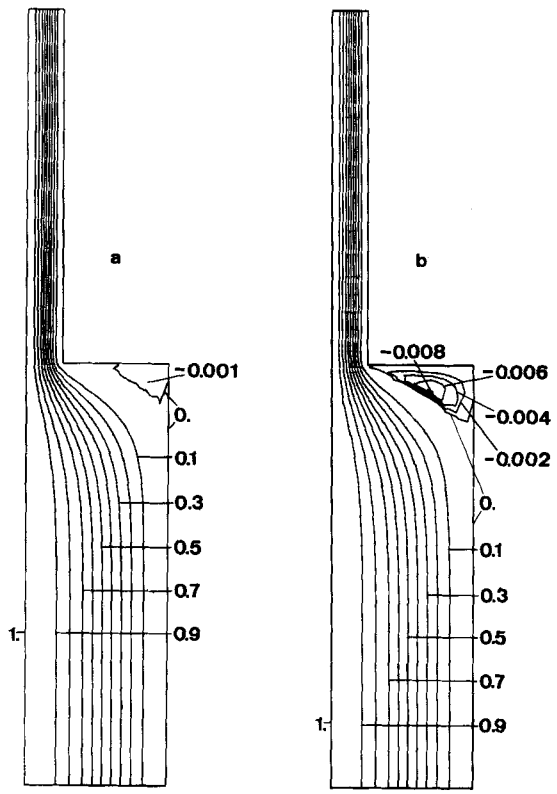

Figure 11. Corner vortex in the axisymmetric contraction: (a) Newtonian case; (b). Maxwell fluid at $S_R = 2{\cdot}4$

$S_R = 3{\cdot}6$. However, using a Phan Thien–Tanner model, Keunings and Crochet[15] have been able to observe an important growth of the vortex size.

The problem of the flow of a Maxwell fluid through an abrupt 4/1 contraction has been run with the method MIX4 on the mesh used in Reference 13; we replace however the composite quadrilaterals used in Reference 13 by Lagrangian quadrilaterals. The mesh, shown in Figure 10, contains 129 elements and 577 nodes, giving rise to 1959 nodal variables. The velocity components

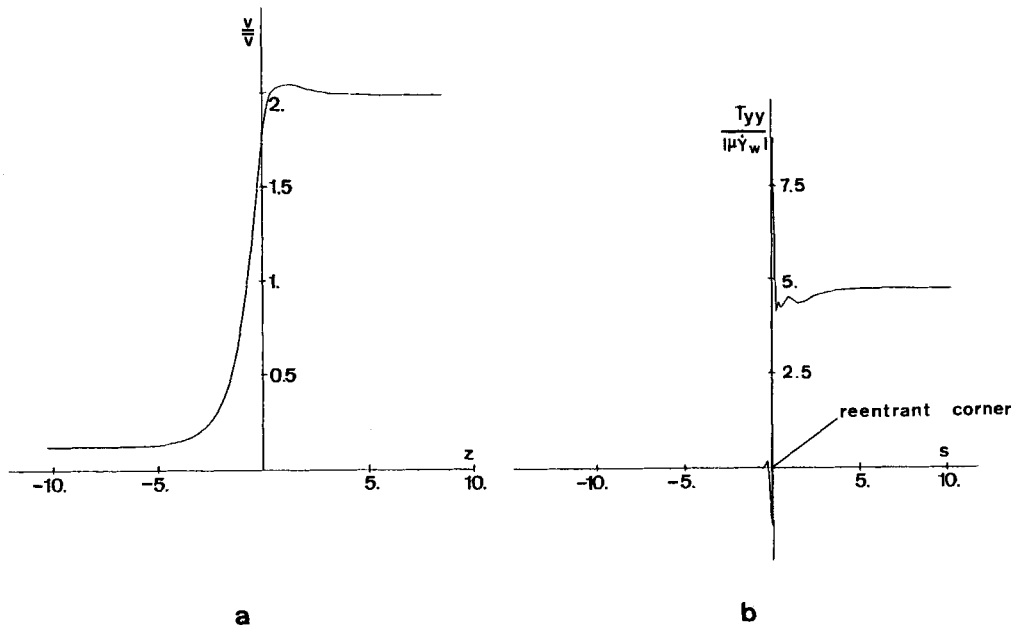

Figure 12. (a) Graph of the axial velocity profile along the axis of symmetry; (b) Graph of the T_{yy} extra-stress component along the wall

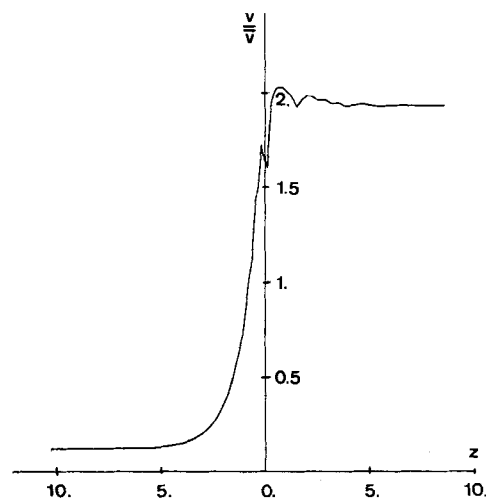

Figure 13. Graph of the axial velocity profile along the axis of symmetry obtained with MIX3

and the extra stresses are imposed in the entry section, whereas the velocity components alone are imposed in the exit section.

The value of $S_R = \lambda \dot{\gamma}_W$ is calculated on the wall of the downstream channel. With the method MIX4, it has been possible to reach a value of $S_R = 2{\cdot}4$, beyond which Newton's method does not converge. The streamlines at $S_R = 2{\cdot}4$ are compared in Figure 11 with those of the Newtonian case; one observes a slight vortex growth which may not be considered as significant. Figure 12(a) shows the development of the axial velocity profile along the axis of the contraction, also at $S_R = 2{\cdot}4$. The velocity profile shows a slight overshoot of 3·0 per cent with respect to the fully developed value, which is in good agreement with the results found in Reference 14 with an Oldroyd-B fluid, where 3·3 per cent was found at $S_R = 2{\cdot}7$. Figure 12(b) reveals the most probable reason for the lack of convergence beyond $S_R = 2{\cdot}4$; it shows the value of T_{yy} along the wall of the contraction, in the neighbourhood of the re-entrant corner. The inherent stress singularity is incompatible with the C^0-approximation used for the extra-stress field; still, a high and narrow stress peak is obtained in the neighbourhood of the corner. The reason why the use of an Oldroyd-B fluid allows the attainment of a higher value of S_R may be that the intensity of the singularity is of a lower order for such a fluid. The method MIX4 has also been run on another finite element mesh for the abrupt 4/1 contraction, which is denser in general than the mesh of Figure 10, but where the elements around the reentrant corner are somewhat larger; it is then possible to reach a value of $S_R = 3{\cdot}4$.

Finally, we wish to show the counterpart of Figure 12(a) obtained with MIX3 at $S_R = 2{\cdot}4$; Figure 13 shows the graph of the axial velocity obtained along the axis with that method. The calculation was not pursued above $S_R = 2{\cdot}4$ in view of the degeneracy of the solution.

8. CONCLUSIONS

Four finite element methods developed for solving the flow of viscoelastic fluids have been applied for solving the same problem. Beyond some critical value of the recoverable shear, all techniques develop spurious wiggles in the velocity field and, above all, in the extra-stress field. The critical value of S_R depends, however, upon the method. It is found that the presence of explicit viscous terms together with the absence of stress gradients in the discretized momentum equations considerably improves the behaviour of the algorithm.

ACKNOWLEDGEMENTS

The research of J. J. Van Schaftingen is sponsored by the 'Fonds National de la Recherche Scientifique', which is gratefully acknowledged.

REFERENCES

1. M. J. Crochet and K. Walters, 'Numerical methods in non-Newtonian fluid mechanics, *Ann. Rev. Fluid Mech.*, **15**, 241–260 (1983).
2. J. G. Oldroyd, 'On the formulation of rheological equations of state', *Proc. R. Soc. London Ser. A*, **200**, 523–541 (1950).
3. M. Kawahara and N. Takeuchi, 'Mixed finite element method for analysis of viscoelastic fluid flow', *Comp. Fluids*, **5**, 33–45 (1977).
4. M. G. N. Perera and K. Walters, 'Long-range memory effects in flows involving abrupt changes in geometry. Part I. Flows associated with L-shaped and T-shaped geometries', *J. Non-Newt. Fluid Mech.*, **2**, 49–81 (1977).
5. M. J. Crochet, 'The flow of a Maxwell fluid around a sphere', in R. H. Gallagher (ed.), *Finite elements in fluids*, Vol. 4, Wiley, 1982, pp. 573–597.
6. C. J. Coleman, 'A finite element routine for analysing non-Newtonian flows. Part 1. Basic method and preliminary results', *J. Non-Newt. Fluid Mech.*, **7**, 289–301 (1980).
7. N. A. Jackson and B. A. Finlayson, 'Calculation of hole pressure II. Viscoelastic fluids', *J. Non-Newt. Fluid Mech.*, **10**, 71–84 (1982).

8. G. D. Richards and P. Townsend, 'A finite element computer model of the hole pressure problem', *Rheol. Acta*, **20**, 261–269 (1981).
9. M. A. Mendelson, P. W. Yeh, R. A. Brown, R. C. Armstrong, 'Aproximation error in finite element calculation of viscoelastic fluid flow', *J. Non-Newt. Fluid Mech.*, **10**, 31–52 (1982).
10. M. J. Crochet and R. Keunings, 'Finite element analysis of die swell of a highly elastic fluid', *J. Non-Newt. Fluid Mech.*, **10**, 339–356 (1982).
11. H. Giesekus, 'Nicht-lineare Effekte beim Strömen viskoelastischer Flüssigkeiten durch Schlitz- und Lochdüsen', *Rheol. Acta*, **7**, 127–138 (1968).
12. J. G. Oldroyd, 'Non-Newtonian flow in liquids and solids', in *Rheology*, vol. 1, Academic Press, 1956, pp. 653–682.
13. M. Viriyayuthakorn and B. Caswell, 'Finite element simulation of viscoelastic flow', *J. Non-Newt. Fluid Mech.*, **6**, 245–267 (1980).
14. M. J. Crochet, 'Numerical simulation of die-entry and die-exit flow of a viscoelastic fluid', in J. F. T. Pittman (ed.), '*Numerical Methods in Industrial Forming Processes*, Pineridge Press, 1982, pp. 85–94.
15. R. Keunings and M. J. Crochet, 'Numerical simulation of the flow of a viscoelastic fluid through an abrupt contraction', *J. Non-Newt. Fluid Mech.*, **14**, 279–299 (1984).